In-gap states of a quantum dot coupled between a normal and a superconducting lead

2013 J. Phys.: Condens. Matter 25 435305

(http://iopscience.iop.org/0953-8984/25/43/435305)

IOP PUBLISHING JOURNAL OF PHYSICS: CONDENSED MATTER
J. Phys.: Condens. Matter **25** (2013) 435305 (9pp) doi:10.1088/0953-8984/25/43/435305

In-gap states of a quantum dot coupled between a normal and a superconducting lead

J Barański and T Domański

Institute of Physics, M Curie-Skłodowska University, 20-031 Lublin, Poland

Received 6 August 2013, in final form 12 September 2013
Published 9 October 2013
Online at stacks.iop.org/JPhysCM/25/435305

Abstract
We study the in-gap states of a quantum dot hybridized with one conducting and another superconducting electrode. The proximity effect suppresses the electronic states in the entire subgap regime $|\omega| < \Delta$, where Δ denotes the energy gap of the superconductor. The Andreev scattering mechanism can induce, however, some in-gap states whose line-broadening (inverse life-time) is controlled by the hybridization of the quantum dot with the normal electrode. We show that the number of such Andreev bound states is substantially dependent on the competition between the Coulomb repulsion and the induced on-dot pairing. We discuss the signatures of these in-gap states in the tunneling conductance, especially in a low-bias regime.

(Some figures may appear in colour only in the online journal)

1. Motivation

Quantum impurities embedded in superconducting host materials have been a topic of intensive study for about 50 years (see the review paper [1]). Early work predominantly explored the way in which impurities affect the superconducting states of bulk materials. It has been established (by the Anderson theorem [2]) that paramagnetic impurities are rather inefficient in isotropic superconductors or eventually weakly suppress the anisotropic superconducting phases [3]. Magnetic (spinful) impurities, in contrast, proved to have much stronger influence on the superconductivity. They induce in-gap states [4] and with increasing concentration of magnetic impurities the energy gap of a superconducting material is gradually filled in, simultaneously suppressing its critical temperature. On a microscopic level this detrimental effect comes from the pair-breaking character of the spin scattering.

The mutual relationship between quantum impurities and superconducting materials is currently again attracting substantial interest due to intensive studies of nanoscopic devices, where various artificial quantum impurities (dots) are connected to external superconducting electrodes. In this context, the main problem refers to the question of how the superconducting reservoirs affect the quantum dots (QDs) rather than the other way around. Due to the proximity effect Cooper pairs can penetrate the quantum dot, converting it into a sort of 'superconducting grain'. On the other hand, the strong Coulomb repulsion between opposite spin electrons disfavors any double (or even) occupancy of the quantum dot. At low temperatures the Kondo physics additionally comes into the play. Both of these phenomena, i.e. Coulomb blockade and the appearance of a Kondo singlet state, strongly compete with the induced on-dot pairing. In nanoscopic tunneling junctions this competition can be explored in a controllable manner, by (a) varying the QD hybridization with the superconducting lead, (b) altering the energy gap $\Delta = \Delta(B)$ by applying a magnetic field B [5], (c) raising the discrete QD energy levels via the gate voltage, and (d) lowering the temperature to activate the Kondo physics. Numerous theoretical and experimental studies of quantum dots connected to superconducting leads have been summarized, e.g., in [6, 7].

The interplay between the on-dot pairing and the correlation effects can be conveniently investigated in a setup where the quantum dot is placed between one superconducting (S) and another normal (N) electrode. In the subgap regime ($eV < \Delta$) the tunneling conductance almost entirely originates from the anomalous Andreev channel; such spectroscopy can thus directly probe any

in-gap states. In experimental realizations of N–QD–S junctions the role of the quantum dots has been played by self-assembled InAs nanoscopic islands [8], carbon nanotubes [9], quantum wires [10], etc. For instance, the use of InAs quantum dots coupled between metallic (gold) and superconducting (aluminum) electrodes provided clear evidence for the Kondo effect coexisting with the induced on-dot pairing manifested by the zero-bias enhancement of the zero-bias Andreev conductance [8]. Tunneling conductance has also recently been measured in a system comprising indium antimonide nanowires connected to a normal (gold) and a superconducting (niobium titanium nitride) electrode, indicating Majorana-type in-gap states [10].

Other measurements have been made using three-terminal configurations with the metallic and superconducting electrodes interconnected via double quantum dots to achieve a controllable Cooper pair splitting. These dots served as 'quantum forks', where the Coulomb repulsion forced electrons (released from the Cooper pairs) to move into different normal leads, while preserving their entanglement. Such a transport channel contributed about 10% for the case of InAs quantum dots [18] and nearly 50% using carbon nanotubes [19] to the total differential conductance. For the latter case the efficiency has been subsequently considerably improved [20]. Experimental measurements have also probed the spin-polarized Andreev current using a ferromagnetic electrode coupled via a quantum dot to a superconducting lead [21]. In all these and many other related experiments [22, 23] the subgap electron transport is solely provided by the in-gap states. Detailed knowledge of these states seems thus to be a timely and important issue.

It is our intention here to gather systematic information on the in-gap Andreev states originating from scattering on either magnetic or non-magnetic quantum impurities. The physical aspects of such a study have been so far addressed by a number of groups using various techniques [6]. Since this problem is currently important [11, 12] we would like to collect the essential results into this single report. Subgap states of magnetic (Kondo-type) impurities have been extensively investigated, both theoretically [13] and experimentally using two-terminal [14] as well as three-terminal configurations [23]. We would like to emphasize, however, that in-gap states are present also in the case of uncorrelated (spinless) quantum dots [15–17]. To illustrate this possibility, in section 3 we briefly analyze a noninteracting quantum dot, considering the evolution of the Andreev bound states with respect to Δ/Γ_S (where Γ_β denotes the coupling to $\beta = N, S$ lead) for several asymmetric coupling ratios Γ_S/Γ_N. Next, in sections 4 and 5, we address the correlation effects responsible for the Coulomb blockade and the Kondo effect.

Our study can be regarded as complementary to the previous pedagogical analysis by Bauer *et al* [15] who focused on the in-gap states of a quantum impurity immersed in a superconducting medium for the limit $\Gamma_S \gg \Delta$. We hope that this analysis will be useful for tunneling spectroscopy using quantum dots asymmetrically coupled between superconducting and normal leads in two- and multi-terminal configurations.

2. The Anderson impurity model

For the description of a quantum dot coupled between normal (N) and superconducting (S) electrodes we use the Anderson impurity model

$$\hat{H} = \hat{H}_N + \hat{H}_S + \sum_\sigma \epsilon_d \hat{d}_\sigma^\dagger \hat{d}_\sigma + U_d \hat{n}_{d\uparrow}\hat{n}_{d\downarrow} + \sum_{\mathbf{k},\sigma}\sum_{\beta=N,S}\left(V_{\mathbf{k}\beta}\,\hat{d}_\sigma^\dagger \hat{c}_{\mathbf{k}\sigma\beta} + V_{\mathbf{k}\beta}^*\,\hat{c}_{\mathbf{k}\sigma,\beta}^\dagger \hat{d}_\sigma\right). \quad (1)$$

The operators d_σ ($d_\sigma^\dagger$) denote annihilation (creation) of a QD electron with spin σ and energy level ε_d and U_d is the on-dot repulsion (or charging) energy. The last term in (1) represents the hybridization of the QD with the external leads, where the normal electrode is described by the Fermi gas $\hat{H}_N = \sum_{\mathbf{k},\sigma}\xi_{\mathbf{k}N}\hat{c}_{\mathbf{k}\sigma N}^\dagger \hat{c}_{\mathbf{k}\sigma N}$ and the superconducting one takes the conventional BCS form $\hat{H}_S = \sum_{\mathbf{k},\sigma}\xi_{\mathbf{k}S}\hat{c}_{\mathbf{k}\sigma S}^\dagger \hat{c}_{\mathbf{k}\sigma S} - \sum_{\mathbf{k}}\Delta(\hat{c}_{\mathbf{k}\uparrow S}^\dagger \hat{c}_{-\mathbf{k}\downarrow S}^\dagger + \hat{c}_{-\mathbf{k}\downarrow S}\hat{c}_{\mathbf{k}\uparrow S})$. The energies $\xi_{\mathbf{k}\beta} = \varepsilon_{\mathbf{k}\beta} - \mu_\beta$ are measured with respect to the chemical potentials μ_β, which can be detuned by the external voltage $\mu_N = \mu_S + eV$. We shall focus on the low energy features, assuming the wide band limit approximation $|V_{\mathbf{k}\beta}| \ll D$ (where $-D \le \varepsilon_{\mathbf{k}\beta} \le D$) and use the coupling constants $\Gamma_\beta = 2\pi\sum_{\mathbf{k},\beta}|V_{\mathbf{k}\beta}|^2\delta(\omega - \xi_{\mathbf{k}\beta})$ as useful energy units.

To consider the proximity effect we introduce the matrix Green's function $\boldsymbol{G}_d(\tau,\tau') = \langle\langle\hat{\Psi}_d(\tau); \hat{\Psi}_d^\dagger(\tau')\rangle\rangle$ in the Nambu representation $\hat{\Psi}_d^\dagger = (\hat{d}_\uparrow^\dagger, \hat{d}_\downarrow)$, $\hat{\Psi}_d = (\hat{\Psi}_d^\dagger)^\dagger$. Under equilibrium conditions the Green's function $\boldsymbol{G}_d(\tau,\tau')$ depends only on the time difference $\tau - \tau'$. Its Fourier transform obeys the following Dyson equation:

$$\boldsymbol{G}_d(\omega)^{-1} = \begin{pmatrix}\omega - \varepsilon_d & 0\\ 0 & \omega + \varepsilon_d\end{pmatrix} - \boldsymbol{\Sigma}_d^0(\omega) - \boldsymbol{\Sigma}_d^U(\omega), \quad (2)$$

where the selfenergy $\boldsymbol{\Sigma}_d^0$ corresponds to the noninteracting case ($U = 0$) and the second contribution $\boldsymbol{\Sigma}_d^U$ refers to the correlation effects induced by the local Coulomb repulsion $U_d\hat{n}_{d,\uparrow}\hat{n}_{d,\downarrow}$. The uncorrelated quantum dot is characterized by

$$\boldsymbol{\Sigma}_d^0(\omega) = \sum_{\mathbf{k},\beta}\left|V_{\mathbf{k}\beta}\right|^2 \boldsymbol{g}_\beta(\mathbf{k},\omega), \quad (3)$$

where $\boldsymbol{g}_N(\mathbf{k},\omega)$ is the Green's function of the normal lead

$$\boldsymbol{g}_N(\mathbf{k},\omega) = \begin{pmatrix}\dfrac{1}{\omega - \xi_{\mathbf{k}N}} & 0\\ 0 & \dfrac{1}{\omega + \xi_{\mathbf{k}N}}\end{pmatrix} \quad (4)$$

and $\boldsymbol{g}_S(\mathbf{k},\omega)$ denotes the Green's function of the superconducting electrode

$$\boldsymbol{g}_S(\mathbf{k},\omega) = \begin{pmatrix}\dfrac{u_\mathbf{k}^2}{\omega - E_\mathbf{k}} + \dfrac{v_\mathbf{k}^2}{\omega + E_\mathbf{k}} & \dfrac{-u_\mathbf{k}v_\mathbf{k}}{\omega - E_\mathbf{k}} + \dfrac{u_\mathbf{k}v_\mathbf{k}}{\omega + E_\mathbf{k}}\\ \dfrac{-u_\mathbf{k}v_\mathbf{k}}{\omega - E_\mathbf{k}} + \dfrac{u_\mathbf{k}v_\mathbf{k}}{\omega + E_\mathbf{k}} & \dfrac{u_\mathbf{k}^2}{\omega + E_\mathbf{k}} + \dfrac{v_\mathbf{k}^2}{\omega - E_\mathbf{k}}\end{pmatrix}. \quad (5)$$

The quasiparticle energies are given by $E_{\mathbf{k}} = \sqrt{\xi_{\mathbf{k}S}^2 + \Delta^2}$ and the usual BCS coefficients take the form $u_{\mathbf{k}}^2$, $v_{\mathbf{k}}^2 = \frac{1}{2}[1 \pm \frac{\xi_{\mathbf{k}S}}{E_{\mathbf{k}}}]$, $u_{\mathbf{k}}v_{\mathbf{k}} = \frac{\Delta}{2E_{\mathbf{k}}}$. In the wide band limit the selfenergy (3) simplifies to

$$\boldsymbol{\Sigma}_{\mathrm{d}}^{0}(\omega) = -\mathrm{i}\frac{\Gamma_{\mathrm{N}}}{2}\begin{pmatrix}1 & 0\\ 0 & 1\end{pmatrix} - \frac{\Gamma_{\mathrm{S}}}{2}\gamma(\omega)\begin{pmatrix}1 & \frac{\Delta}{\omega}\\ \frac{\Delta}{\omega} & 1\end{pmatrix} \tag{6}$$

with ω-dependent function

$$\gamma(\omega) = \begin{cases} \dfrac{\omega}{\sqrt{\Delta^2-\omega^2}} & \text{for } |\omega| < \Delta, \\ \dfrac{\mathrm{i}\,|\omega|}{\sqrt{\omega^2-\Delta^2}} & \text{for } |\omega| > \Delta. \end{cases} \tag{7}$$

To consider the correlation effects $\Sigma_{\mathrm{d}}^{U}(\omega)$ one has to introduce some approximations. We shall come back to this non-trivial problem in sections 4 and 5.

3. In-gap states of an uncorrelated quantum dot

Let us start by considering an uncorrelated QD, which is equivalent to a spinless impurity. We discuss here the spectroscopic properties of such a QD for an arbitrary ratio $\Delta/\Gamma_{\mathrm{S}}$ and asymmetric couplings $\Gamma_{\mathrm{N}} \neq \Gamma_{\mathrm{S}}$. In-gap states formally represent the poles of the matrix Green's function $\boldsymbol{G}_{\mathrm{d}}(\omega)$ existing in the subgap regime $|\omega| < \Delta$. For an uncorrelated quantum dot ($U_{\mathrm{d}} \to 0$) one has

$$\boldsymbol{G}_{\mathrm{d}}(\omega) = \frac{1}{(\tilde{\omega}+\mathrm{i}\frac{\Gamma_{\mathrm{N}}}{2})^2 - \varepsilon_{\mathrm{d}}^2 - (\frac{\tilde{\Gamma}_{\mathrm{S}}}{2})^2} \times \begin{pmatrix}\tilde{\omega}+\mathrm{i}\dfrac{\Gamma_{\mathrm{N}}}{2}+\varepsilon_{\mathrm{d}} & -\dfrac{\tilde{\Gamma}_{\mathrm{s}}}{2}\\ -\dfrac{\tilde{\Gamma}_{\mathrm{s}}}{2} & \tilde{\omega}+\mathrm{i}\dfrac{\Gamma_{\mathrm{N}}}{2}-\varepsilon_{\mathrm{d}}\end{pmatrix} \tag{8}$$

with the following meaning of the symbols $\tilde{\omega}$ and $\tilde{\Gamma}_{\mathrm{S}}$:

$$\tilde{\omega} = \omega + \frac{\Gamma_{\mathrm{S}}}{2}\frac{\omega}{\sqrt{\Delta^2-\omega^2}}, \tag{9}$$

$$\tilde{\Gamma}_{\mathrm{s}} = \Gamma_{\mathrm{S}}\frac{\Delta}{\sqrt{\Delta^2-\omega^2}}. \tag{10}$$

In this case the single-particle spectral function $\rho_{\mathrm{d}}(\omega) \equiv -\frac{1}{\pi}\mathrm{Im}\left\{\boldsymbol{G}_{\mathrm{d},11}(\omega)\right\}$ is expressed by the standard BCS form

$$\boldsymbol{G}_{\mathrm{d},11}(\omega) = \frac{1}{2}\left[1+\frac{\varepsilon_{\mathrm{d}}}{\tilde{E}_{\mathrm{d}}}\right]\frac{1}{\tilde{\omega}+\mathrm{i}\frac{\Gamma_{\mathrm{N}}}{2}-\tilde{E}_{\mathrm{d}}} + \frac{1}{2}\left[1-\frac{\varepsilon_{\mathrm{d}}}{\tilde{E}_{\mathrm{d}}}\right]\frac{1}{\tilde{\omega}+\mathrm{i}\frac{\Gamma_{\mathrm{N}}}{2}+\tilde{E}_{\mathrm{d}}} \tag{11}$$

with ω-dependent parameter

$$\tilde{E}_{\mathrm{d}} = \sqrt{\varepsilon_{\mathrm{d}}^2 + (\tilde{\Gamma}_{\mathrm{s}}/2)^2}. \tag{12}$$

In figure 1 we show the spectrum $\rho_{\mathrm{d}}(\omega)$ as a function of the energy gap Δ obtained for an uncorrelated (spinless) quantum dot with $\varepsilon_{\mathrm{d}} = 0$ and $-\Gamma_{\mathrm{S}}$. We have assumed a weak coupling to the normal lead $\Gamma_{\mathrm{N}} \ll \Gamma_{\mathrm{S}}$, which yields a nearly resonant character of the in-gap states. For larger Γ_{N} the in-gap state broadening increases (the life-time decreases). We furthermore notice (see figure 2) that Andreev states appear near the gap edge singularities (for $\Delta \ll \Gamma_{\mathrm{S}}$) and they evolve into subgap peaks centered at energies $\pm\sqrt{\varepsilon_{\mathrm{d}}^2 + \Gamma_{\mathrm{S}}^2/4}$ (for $\Delta \gg \Gamma_{\mathrm{S}}$).

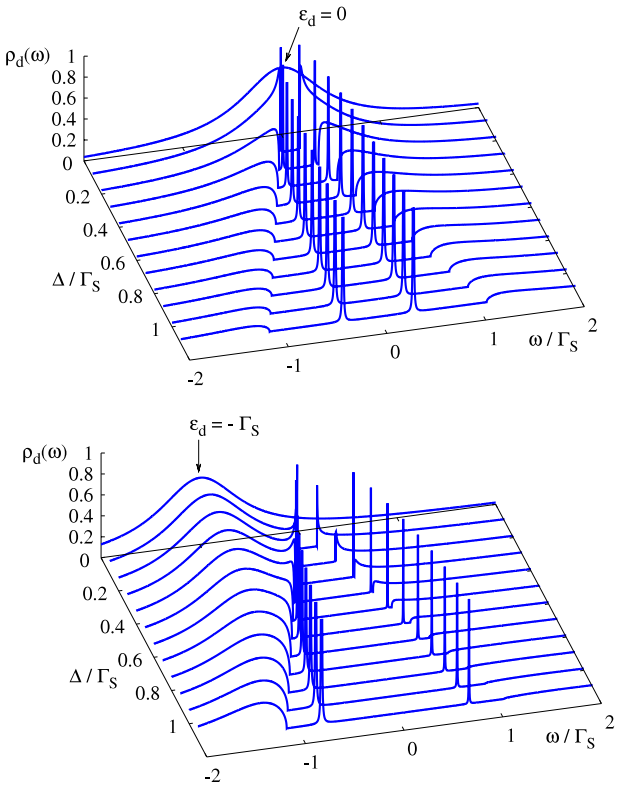

Figure 1. The spectral function $\rho_{\mathrm{d}}(\omega)$ of an uncorrelated quantum dot obtained for $\varepsilon_{\mathrm{d}} = 0$ (upper panel) and $\varepsilon_{\mathrm{d}} = -\Gamma_{\mathrm{S}}$ (bottom panel) assuming weak coupling to the metallic lead, $\Gamma_{\mathrm{N}} = 0.001\Gamma_{\mathrm{S}}$. In both cases the in-gap states gradually emerge from the gap edge singularities $\pm\Delta$ (when $\Delta \ll \Gamma_{\mathrm{S}}$) and they evolve to well-defined subgap quasiparticle peaks (when $\Delta \gg \Gamma_{\mathrm{S}}$).

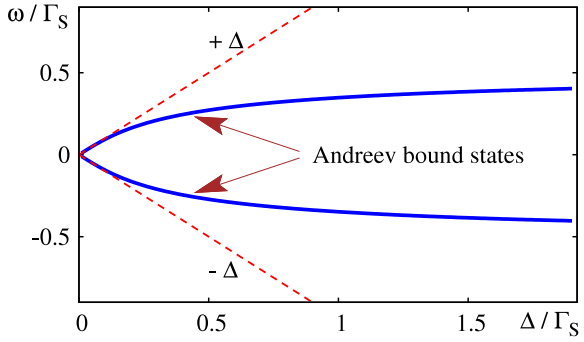

Figure 2. The energies of the in-gap states versus the ratio $\Delta/\Gamma_{\mathrm{S}}$ obtained for an uncorrelated quantum dot ($\varepsilon_{\mathrm{d}} = 0$) weakly coupled to a metallic lead $\Gamma_{\mathrm{N}} = 0.001\Gamma_{\mathrm{S}}$. The dashed lines indicate the gap edges $\pm\Delta$.

3.1. Resonances in the weak coupling limit $\Gamma_N \to 0$

To get some correspondence with the previous study [15] we now consider in more detail the case of infinitesimally weak coupling to the normal electrode, $\Gamma_N \to 0^+$. Under such a condition the in-gap states become strictly resonant, i.e. they represent the quasiparticles of an infinite life-time. In the subgap regime equation (12) yields the following spectral function:

$$\lim_{|\omega|<\Delta} \rho_d(\omega) = \frac{1}{2}\left(1+\frac{\varepsilon_d}{\tilde{E}_d}\right)\delta\left[\tilde{\omega}-\tilde{E}_d\right] + \frac{1}{2}\left(1-\frac{\varepsilon_d}{\tilde{E}_d}\right)\delta\left[\tilde{\omega}+\tilde{E}_d\right]. \quad (13)$$

This function can be rewritten as

$$\lim_{|\omega|<\Delta} \rho_d(\omega) = \mathcal{W}_+\,\delta\left[\omega-E_+\right] + \mathcal{W}_-\,\delta\left[\omega-E_-\right] \quad (14)$$

with the quasiparticle energies $E_\pm$ representing the solutions of the following equation:

$$E_\pm + \frac{\Gamma_S}{2}\frac{E_\pm}{\sqrt{\Delta^2-E_\pm^2}} = \pm\sqrt{\varepsilon_d^2+\left(\frac{\Gamma_S}{2}\right)^2\frac{\Delta^2}{\Delta^2-E_\pm^2}} \quad (15)$$

and $\mathcal{W}_\pm$ being their spectral weights.

We illustrate in figure 2 the energies $E_\pm$ of the in-gap resonances versus the ratio Δ/Γ_S obtained for $\varepsilon_d = 0$. In the case of a small energy gap $\Delta \ll \Gamma_S$ (studied by Bauer *et al* [15]) the resonant in-gap states are located near the gap edge singularities $\pm\Delta$. For increasing Δ/Γ_S they gradually move away from the gap edge singularities, and in the limit $\Delta \gg \Gamma_S$ they approach the asymptotic values $\pm\sqrt{\varepsilon_d+(\Gamma_S/2)^2}$. In section 3.2 we discuss in more detail this 'superconducting atomic' limit $\Delta \gg \Gamma_S$.

3.2. The superconducting atomic limit $\Delta \gg \Gamma_S$

Deep inside the energy gap (i.e. for $|\omega| \ll \Delta$) all electronic states of the uncorrelated quantum dot can be determined analytically (for arbitrary Γ_β) due to the fact that the selfenergy (6) simplifies then to a static value

$$\boldsymbol{\Sigma}_d^0(\omega) = -\tfrac{1}{2}\begin{pmatrix} i\Gamma_N & \Gamma_S \\ \Gamma_S & i\Gamma_N \end{pmatrix}. \quad (16)$$

Under such conditions the quantum dot can be regarded as a 'superconducting island' with an induced pairing gap $\Delta_d = |\Gamma_S/2|$. This problem has been widely discussed in the literature, adopting various methods to describe the correlation effects U_d (see sections 4 and 5).

The spectral function $\rho_d(\omega)$ of the uncorrelated QD can be expressed explicitly by

$$\rho_d(\omega) = \frac{1}{2}\left[1+\frac{\varepsilon_d}{E_d}\right]\frac{\frac{1}{\pi}\Gamma_N/2}{(\omega-E_d)^2+(\Gamma_N/2)^2} + \frac{1}{2}\left[1-\frac{\varepsilon_d}{E_d}\right]\frac{\frac{1}{\pi}\Gamma_N/2}{(\omega+E_d)^2+(\Gamma_N/2)^2} \quad (17)$$

with the quasiparticle energy $E_d = \sqrt{\varepsilon_d^2+\Delta_d^2}$. The subgap spectrum consists thus of the particle and hole peaks at $\omega = \pm E_d$ whose spectral weights depend on ε_d, and the broadening is controlled by Γ_N. These particle and hole Lorentzians are well separated from each other until $\Gamma_S \geq \Gamma_N$. Otherwise, they merge into a single structure (see the second reference of [38]).

3.3. Tunneling spectroscopy

Any experimental verification of the subgap states is possible only indirectly, by measuring the differential conductance of the tunneling current $I(V)$. In general, the charge transport induced through an N–QD–S junction consists of the quasiparticle (QP) and Andreev (A) currents $I(V) = I_{QP}(V) + I_A(V)$. They can expressed in the Landauer-type form [32]

$$I_{QP}(V) = \frac{2e}{h}\int d\omega\, T_{QP}(\omega)\,[f(\omega-eV)-f(\omega)], \quad (18)$$

$$I_A(V) = \frac{2e}{h}\int d\omega\, T_A(\omega)\,[f(\omega-eV)-f(\omega+eV)] \quad (19)$$

with the Fermi distribution $f(\omega) = \left[\exp(\omega/k_BT)+1\right]^{-1}$. The transmittance of the Andreev channel $T_A(\omega)$ depends on the off-diagonal part of the Green's function

$$T_A(\omega) = |\Gamma_N|^2\,\left|\boldsymbol{G}_{d,12}(\omega)\right|^2, \quad (20)$$

whereas the effective quasiparticle transmittance $T_{QP}(\omega)$ contains several contributions

$$T_{QP}(\omega) = \Gamma_N\Gamma_S\left(|\boldsymbol{G}_{d,11}(\omega)|^2+|\boldsymbol{G}_{d,12}(\omega)|^2 - \frac{\Delta}{\omega}\mathrm{Re}\{\boldsymbol{G}_{d,11}(\omega)\boldsymbol{G}_{d,12}^*(\omega)\}\right). \quad (21)$$

Usually the off-diagonal Green's function $\boldsymbol{G}_{d,12}(\omega)$ quickly vanishes outside the energy gap; therefore for $|\omega| \geq \Delta$ the tunneling current simplifies to the popular Meir–Wingreen formula

$$\lim_{|eV|\geq\Delta} I(V) \approx \frac{2e}{h}\int d\omega\,\Gamma_N\Gamma_S\,\left|\boldsymbol{G}_{d,11}(\omega)\right|^2 \times [f(\omega-eV)-f(\omega)]. \quad (22)$$

In the subgap regime $|\omega| < \Delta_d$ (especially for strongly asymmetric couplings $\Gamma_S \gg \Gamma_N$) the transport is solely provided by the Andreev current (19). Figure 3 shows the Andreev conductance $G_A(V) = \frac{d}{dV}I_A(V)$ obtained for $\Gamma_N = 0.1\Gamma_S$. We can notice that the differential conductance is similar (although not identical) to the in-gap spectrum $\rho_d(\omega)$ presented in figures 1 and 2.

The next plot, figure 4, illustrates the total conductance $G(V) = \frac{d}{dV}I(V)$ obtained at $T = 0$ for $\varepsilon_d = -2\Gamma_S$. In these curves we can clearly identify (a) the broad peak at $eV = \varepsilon_d$, (b) the signatures of gap edge singularities (manifested by sharp enhancement of the single-particle tunneling at $eV = \pm\Delta$), and (c) the well pronounced in-gap features related to the Andreev bound states. For $\Delta > \Gamma_S$ the in-gap features are well separated from the gap edge singularities, otherwise it is

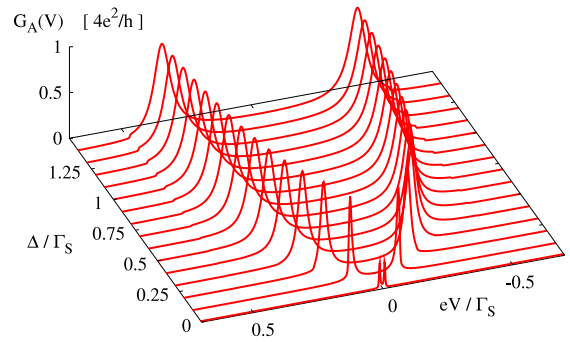

Figure 3. The subgap Andreev conductance obtained for an uncorrelated quantum dot with $\varepsilon_d = 0$ and asymmetric couplings $\Gamma_N/\Gamma_S = 0.1$.

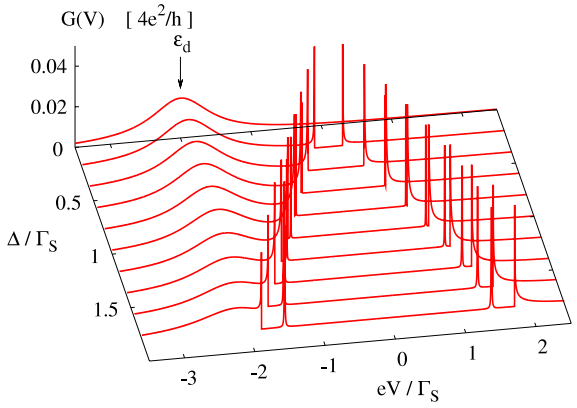

Figure 4. The effective differential conductance of an uncorrelated quantum dot asymmetrically coupled to external leads $\Gamma_N/\Gamma_S = 0.01$ obtained for $\varepsilon_d = -2\Gamma_S$.

rather difficult to recognize them for the coupling $\Gamma_N \geq \Gamma_S$ (for instance, see figure 2 in [13]). The experimental data of Deacon *et al* [8] clearly confirmed such well-defined subgap peaks in the Andreev conductance for the strongly asymmetric coupling $\Gamma_S \geq 40\Gamma_N$.

4. Correlation effects

The interplay between the Coulomb repulsion and the induced on-dot pairing is, in general, a very complicated issue. To gain some insight regarding their competition we shall consider the strongly asymmetric limit $\Gamma_S \gg \Gamma_N$ (i.e. assuming $\Gamma_N = 0^+$). In the absence of Coulomb repulsion the strong hybridization to the superconducting electrode converts the quantum dot into a 'superconducting impurity' with the induced pairing gap $\Delta_d = \Gamma_S/2$. The influence of the Coulomb repulsion U_d on the subgap Andreev states in the large gap limit with vanishing coupling to the normal lead was first addressed by Vecino *et al* [24]. Comparison of the methods used for determination of the bound states of the 'superconducting Anderson model' has recently been revisited in [25]. In what follows, we briefly summarize the essential results based on the exact solution of the effective 'superconducting' QD Hamiltonian [26]

$$\hat{H}_{QD} = \sum_\sigma \varepsilon_d \hat{d}^\dagger_\sigma \hat{d}_\sigma - \Delta_d \left(\hat{d}^\dagger_\uparrow \hat{d}^\dagger_\downarrow + \hat{d}_\downarrow \hat{d}_\uparrow \right) + U \hat{n}_{d\downarrow} \hat{n}_{d\uparrow}, \quad (23)$$

where the proximity effect is taken into account by the pair source/sink terms. The doublet configurations $|\uparrow\rangle$ and $|\downarrow\rangle$ (corresponding to total spin $S = \frac{1}{2}$) represent true eigenstates with the eigenvalue ε_d. The other singlet states ($S = 0$) can be expressed as linear combinations of the empty and doubly occupied sites

$$|\Psi_-\rangle = u_d\,|0\rangle - v_d\,|\uparrow\downarrow\rangle\,, \quad (24)$$

$$|\Psi_+\rangle = v_d\,|0\rangle + u_d\,|\uparrow\downarrow\rangle\,. \quad (25)$$

The corresponding eigenenergies are given by [15, 24, 27]

$$E_\mp = \left(\varepsilon_d + \frac{U_d}{2}\right) \mp \sqrt{\left(\varepsilon_d + \frac{U_d}{2}\right)^2 + \Delta_d^2} \quad (26)$$

and the diagonalization coefficients u_d, v_d take the form

$$u_d^2 = \frac{1}{2}\left[1 + \frac{\varepsilon_d + U_d/2}{E_d}\right] = 1 - v_d^2 \quad (27)$$

with $E_d = \sqrt{(\varepsilon_d + U_d/2)^2 + \Delta_d^2}$. Using the spectral Lehmann representation we can determine the full matrix Green's function $\boldsymbol{G}_{QD}(\omega)$ of the 'superconducting atomic limit' (in the case $\Gamma_N = 0^+$). Because of the Coulomb blockade it takes effectively the four-pole structure

$$\boldsymbol{G}_{QD,11}(\omega) = \frac{\alpha\, u_d^2}{\omega - (\frac{U_d}{2} + E_d)} + \frac{\beta\, v_d^2}{\omega - (\frac{U_d}{2} - E_d)} + \frac{\alpha\, v_d^2}{\omega + (\frac{U_d}{2} + E_d)} + \frac{\beta\, u_d^2}{\omega + (\frac{U_d}{2} - E_d)}, \quad (28)$$

$$\boldsymbol{G}_{QD,12}(\omega) = \frac{\alpha\, u_d v_d}{\omega - (\frac{U_d}{2} + E_d)} - \frac{\beta\, u_d v_d}{\omega - (\frac{U_d}{2} - E_d)} - \frac{\alpha\, u_d v_d}{\omega + (\frac{U_d}{2} + E_d)} + \frac{\beta\, u_d v_d}{\omega + (\frac{U_d}{2} - E_d)} \quad (29)$$

and $\boldsymbol{G}_{QD,22}(\omega) = -[\boldsymbol{G}_{QD,11}(-\omega)]^*$, $\boldsymbol{G}_{QD,12}(\omega) = [\boldsymbol{G}_{QD,21}(-\omega)]^*$. The relative spectral weights α and β are given by

$$\alpha = \frac{\exp\{\frac{U_d}{2k_BT}\} + \exp\{-\frac{E_d}{k_BT}\}}{2\,\exp\{\frac{U_d}{2k_BT}\} + \exp\{-\frac{E_d}{k_BT}\} + \exp\{\frac{E_d}{k_BT}\}} = 1 - \beta. \quad (30)$$

The spectrum of the correlated quantum dot consists of the four in-gap resonances at quasiparticle energies $\pm\frac{U_d}{2} \pm E_d$. For arbitrary U_d the spectral function $\rho_{QD}(\omega) \equiv -\frac{1}{\pi}\mathrm{Im}\left\{\boldsymbol{G}_{QD,11}(\omega)\right\}$ takes the following form:

$$\rho_{QD}(\omega) = \alpha u_d^2\, \delta\left(\omega - \frac{U_d}{2} - E_d\right) + \beta v_d^2\, \delta\left(\omega - \frac{U_d}{2} + E_d\right)$$

$$+\alpha v_{\rm d}^2\,\delta\left(\omega+\frac{U_{\rm d}}{2}+E_{\rm d}\right)$$

$$+\beta u_{\rm d}^2\,\delta\left(\omega+\frac{U_{\rm d}}{2}-E_{\rm d}\right). \qquad (31)$$

This spectral function obeys the sum rule $\int_{-\infty}^{\infty}\rho_{\rm QD}(\omega)\,{\rm d}\omega=1$. For $U_{\rm d}=0$ it properly reproduces the exact BCS-type solution $\lim_{U_{\rm d}\to 0}\rho_{\rm QD}(\omega)=u_{\rm d}^2\delta(\omega-\sqrt{\varepsilon_{\rm d}^2+\Delta_{\rm d}^2})+v_{\rm d}^2\delta(\omega+\sqrt{\varepsilon_{\rm d}^2+\Delta_{\rm d}^2})$. Using (23) we can discuss the qualitative effects due to the competition between the Coulomb interactions and the proximity induced on-dot pairing. This aspect has been practically investigated in various nanoscopic setups [8, 11, 12]. Expansions around this 'superconducting atomic limit' (for $\Gamma_{\rm N}\neq 0$) have been developed in [28, 29].

Since the most profound influence of the Coulomb repulsion takes place in the particle–hole symmetric case (i.e. for $\varepsilon_{\rm d}=-U_{\rm d}/2$) we shall explore this situation, focusing on the fate of in-gap resonances upon varying $U_{\rm d}$. The Coulomb potential $U_{\rm d}$ directly affects the quasiparticle energies $\pm U_{\rm d}/2\pm\Delta_{\rm d}$ and their spectral weights. By inspecting (26) we can notice that for $\Delta_{\rm d}=\frac{1}{2}U_{\rm d}$ the ground state evolves from the BCS singlet to the doublet configuration [15]. This crossover is accompanied by significant redistribution of the spectral weights

$$\lim_{T\to 0}\alpha=\begin{cases}0 & \text{for } \frac{1}{2}U_{\rm d}<\Delta,\\ \frac{1}{3} & \text{for } \frac{1}{2}U_{\rm d}=\Delta,\\ \frac{1}{2} & \text{for } \frac{1}{2}U_{\rm d}>\Delta.\end{cases} \qquad (32)$$

In the weak interaction limit $\frac{1}{2}U_{\rm d}<\Delta$ (corresponding to the BCS singlet state) the spectrum consists of two peaks

$$\rho_{\rm QD}(\omega)=\frac{1}{2}\delta\left(\omega-\frac{U_{\rm d}}{2}+\Delta_{\rm d}\right)+\frac{1}{2}\delta\left(\omega+\frac{U_{\rm d}}{2}-\Delta_{\rm d}\right), \qquad (33)$$

separated by an effective energy gap $2\Delta_{\rm d}-U_{\rm d}$. At the singlet–doublet crossover (i.e. for $\frac{1}{2}U_{\rm d}=\Delta$) the spectrum evolves to three-pole structure

$$\rho_{\rm QD}(\omega)=\tfrac{1}{6}\delta(\omega+2\Delta_{\rm d})+\tfrac{1}{6}\delta(\omega-2\Delta_{\rm d})+\tfrac{2}{3}\delta(\omega). \qquad (34)$$

Finally, in the strong interaction limit $\frac{1}{2}U_{\rm d}>\Delta$ (corresponding to the doublet configuration), the spectral function $\rho_{\rm QD}(\omega)$ consists of the four in-gap resonances

$$\rho_{\rm QD}(\omega)=\frac{1}{4}\delta\left(\omega\pm\frac{U_{\rm d}}{2}\pm\Delta_{\rm d}\right). \qquad (35)$$

In the non-symmetric case $\varepsilon_{\rm d}\neq -U_{\rm d}/2$ the singlet–doublet crossover occurs at larger values of $U_{\rm d}$, but still the QP spectrum comprises either two, three, or four subgap Andreev states. We illustrate this behavior in figures 5 and 6, where the coupling $\Gamma_{\rm N}$ to the normal electrode is treated via the simple substitution $\boldsymbol{G}_{\rm d}^{-1}(\omega)=[\boldsymbol{G}_{\rm QD}(\omega)]^{-1}+\frac{\rm i}{2}\Gamma_{\rm N}\boldsymbol{I}$ [27]. The influence of the metallic lead causes then a broadening of the subgap states.

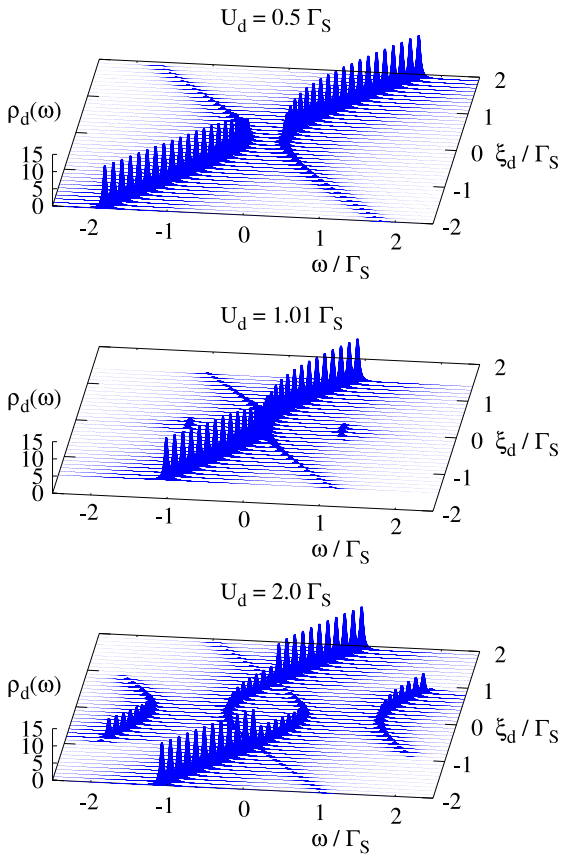

Figure 5. The spectral function $\rho_{\rm d}(\omega)$ of a correlated quantum dot obtained at $T=0$ in the 'superconducting atomic limit' $\Delta\gg\Gamma_S$ for several values of the Coulomb potential $U_{\rm d}$. We plot the spectral function with respect to the energy $\xi_{\rm d}\equiv\varepsilon_{\rm d}+\frac{U_{\rm d}}{2}$ for $U_{\rm d}/\Gamma_{\rm S}=0.5$ (upper panel), 1.01 (middle panel) and 2.0 (lower panel).

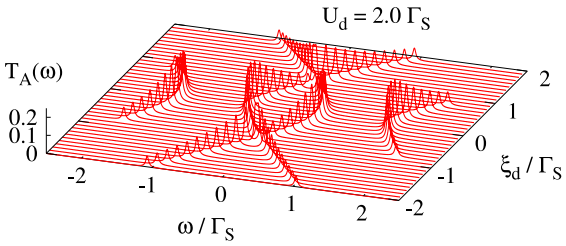

Figure 6. The Andreev transmittance (20) obtained at $T=0$ in the 'superconducting atomic limit' for $U_{\rm d}=2\Gamma_{\rm S}$.

5. Subgap states in the Kondo regime

In this section we address additional effects characteristic for the Kondo regime. This issue has been studied in the literature by a number of authors using a variety of methods, such as the equation of motion technique [30], the slave boson approach [31, 32], the non-crossing approximation [33], iterated perturbation theory [34, 35], the Keldysh Green's function approach combined with the path integral formalism and the dynamical mean field approximation [36], numerical renormalization group [26, 37], the modified equation of motion approach [38], functional renormalization group [39], the cotunneling approach (for a spinful dot) [13], quantum

Monte Carlo simulations [40], and others [41, 42]. In particular, it has been checked whether the Kondo resonance could be somehow manifested in the subgap conductance.

To study the qualitative features caused by the Kondo effect we shall determine the total selfenergy $\mathbf{\Sigma}_{\rm d}(\omega) = \mathbf{\Sigma}_{\rm d}^{0}(\omega) + \mathbf{\Sigma}_{\rm d}^{U}(\omega)$ in the matrix form

$$\mathbf{\Sigma}_{\rm d}(\omega) = \begin{pmatrix} \Sigma_{\uparrow}^{\rm diag}(\omega) & \Sigma^{\rm off}(\omega) \\ [\Sigma^{\rm off}(-\omega)]^{*} & -[\Sigma_{\downarrow}^{\rm diag}(-\omega)]^{*} \end{pmatrix}, \tag{36}$$

focusing on the subgap limit $\Delta \gg \Gamma_{\rm S}$. We thus consider a correlated quantum dot with the induced on-dot pairing $\Delta_{\rm d}$ coupled to a metallic lead $\hat{H} = \sum_{\sigma}\varepsilon_{\rm d}\hat{d}_{\sigma}^{\dagger}\hat{d}_{\sigma} + U\hat{n}_{\rm d\downarrow}\hat{n}_{\rm d\uparrow} - \Delta_{\rm d}(\hat{d}_{\uparrow}^{\dagger}\hat{d}_{\downarrow}^{\dagger} + \hat{d}_{\downarrow}\hat{d}_{\uparrow}) + \hat{H}_{\rm N} + \sum_{\mathbf{k},\sigma}(V_{\mathbf{k}N}\hat{d}_{\sigma}^{\dagger}\hat{c}_{\mathbf{k}\sigma \rm N} + \text{h.c.})$. This simplified problem is not solvable exactly; therefore we have to impose some approximations. For this purpose we treat the Coulomb interactions within the selfconsistent scheme based on the equation of motion (EOM) approach [44] extended to the case of the on-dot pairing $\Delta_{\rm d} \neq 0$.

As a starting point we express the diagonal part of the Green's function $\boldsymbol{G}$ by the BCS-type pairing Ansatz [43]

$$[\boldsymbol{G}_{11}(\omega)]^{-1} = \omega - \varepsilon_{\rm d} - \Sigma_{\uparrow}^{\rm diag}(\omega) - \frac{\Delta_{\rm d}^{2}}{\omega + \varepsilon_{\rm d} + [\Sigma_{\downarrow}^{\rm diag}(-\omega)]^{*}}. \tag{37}$$

The hole propagator is related to (37) via $\boldsymbol{G}_{22}(\omega) = -[\boldsymbol{G}_{11}(-\omega)]^{*}$. Let us notice that in the noninteracting case $\lim_{U_{\rm d}\to 0}\Sigma_{\sigma}^{\rm diag}(\omega) = -{\rm i}\Gamma_{\rm N}/2$. For arbitrary $U_{\rm d} \neq 0$ we estimate $\Sigma_{\sigma}^{\rm diag}(\omega)$ using the EOM decoupling procedure [44] (for details see appendix B in [45]), but our scheme outlined below can be combined also with other approximations, for instance the NCA [33], perturbative expansion [34], etc. The EOM approach yields

$$\Sigma_{\sigma}^{\rm diag}(\omega) \simeq U_{\rm d}\left[n_{{\rm d},\bar{\sigma}} - \Sigma_{1}(\omega)\right] + \frac{U_{\rm d}\left[n_{{\rm d},\bar{\sigma}} - \Sigma_{1}(\omega)\right]\left[\Sigma_{3}(\omega) + U_{\rm d}(1-n_{{\rm d},\bar{\sigma}})\right]}{\omega - \varepsilon_{\rm d} - \Sigma_{0}(\omega) - \left[\Sigma_{3}(\omega) + U_{\rm d}(1-n_{{\rm d},\bar{\sigma}})\right]}, \tag{38}$$

where $\Sigma_{0}(\omega) = -\frac{\rm i}{2}\Gamma_{\rm N}$,

$$\Sigma_{\nu}(\omega) = \sum_{\mathbf{k}}|V_{\mathbf{k}N}|^{2}\left[\frac{1}{\omega - \xi_{\mathbf{k}N}} + \frac{1}{\omega - U_{\rm d} - 2\varepsilon_{\rm d} + \xi_{\mathbf{k}N}}\right] \times \begin{cases} f(\xi_{\mathbf{k}\rm N}) & \text{for } \nu = 1 \\ 1 & \text{for } \nu = 3 \end{cases} \tag{39}$$

and $\bar{\uparrow} = \downarrow$, $\bar{\downarrow} = \uparrow$. To determine the off-diagonal parts of $\boldsymbol{G}(\omega)$ we next use the following exact relation:

$$(\omega - \varepsilon_{\rm d})\boldsymbol{G}_{11}(\omega) = 1 + U_{\rm d}\langle\langle \hat{d}_{\uparrow}\hat{n}_{\rm d\downarrow}; \hat{d}_{\uparrow}^{\dagger}\rangle\rangle - \Delta_{\rm d}\boldsymbol{G}_{12}(\omega) \tag{40}$$

and $\boldsymbol{G}_{21}(\omega) = \boldsymbol{G}_{12}^{*}(-\omega)$. As an approximation we neglect here the influence of the induced on-dot pairing on the two-body propagator $\langle\langle \hat{d}_{\uparrow}\hat{n}_{\rm d\downarrow}; \hat{d}_{\uparrow}^{\dagger}\rangle\rangle$ appearing in (40). This assumption should be justified as long as $U_{\rm d}$ is safely larger than $\Delta_{\rm d} = \Gamma_{\rm S}/2$. We thus take

$$\langle\langle \hat{d}_{\uparrow}\hat{n}_{\rm d\downarrow}; \hat{d}_{\uparrow}^{\dagger}\rangle\rangle \simeq \frac{n_{\rm d\downarrow} - \Sigma_{1}(\omega)\,\boldsymbol{G}_{11}(\omega)}{\omega - \varepsilon_{\rm d} - \Sigma_{0}(\omega) - U_{\rm d} - \Sigma_{3}(\omega)}, \tag{41}$$

which formally originates from the EOM solution [44].

Having this first guess for the matrix Green's function $\boldsymbol{G}(\omega)$ (expressed through equations (37)–(41)) we now construct its selfconsistent improvement. We update the initial pairing Ansatz (37) by iteratively substituting the former selfenergy functional $\mathbf{\Sigma}[\boldsymbol{G}(\omega)]$ into the true relation

$$[\boldsymbol{G}_{11}(\omega)]^{-1} = \omega - \varepsilon_{\rm d} - \Sigma^{\rm diag}(\omega) - \frac{\left[\mathbf{\Sigma}^{\rm off}(-\omega)\right]^{*}\mathbf{\Sigma}^{\rm off}(\omega)}{\omega + \varepsilon_{\rm d} + \left[\Sigma^{\rm diag}(-\omega)\right]^{*}}. \tag{42}$$

At each step we determine the off-diagonal terms via (40) and continue until a satisfactory convergence is reached. We have made numerical calculations of the matrix Green's function $\boldsymbol{G}(\omega)$ within such an algorithm using a mesh of 9000 equidistant energies ω_{n} slightly above the real axis. We have noticed that, in practice, 7–11 iterations are sufficient for a good convergence.

Let us remark that upon neglecting the terms $\Sigma_{1}(\omega)$ and $\Sigma_{3}(\omega)$ of the diagonal selfenergy (38) in the initial iterative step we would recover the usual second order perturbation formula $\lim_{\Sigma_{1},\Sigma_{3}\to 0}\Sigma_{\sigma}^{\rm diag}(\omega) = U_{\rm d}n_{{\rm d},\bar{\sigma}} + U_{\rm d}^{2}\frac{n_{{\rm d},\bar{\sigma}}(1-n_{{\rm d},\bar{\sigma}})}{\omega + {\rm i}\Gamma_{\rm N}/2 - \varepsilon_{\rm d} - U_{\rm d}(1-n_{{\rm d},\bar{\sigma}})}$. This fact indicates that such a simplified selfenergy is able to account for the charging effect (i.e. the Coulomb blockade) discussed by us in section 4. In our numerical treatment we keep, however, all the contributions entering (38) because they are important in the Kondo regime $\varepsilon_{\rm d} < 0 < \varepsilon_{\rm d} + U_{\rm d}$. At temperatures below $k_{\rm B}T_{\rm K} = 0.5\sqrt{U_{\rm d}\Gamma_{\rm N}}\exp\{-\pi\frac{|\varepsilon_{\rm d}(\varepsilon_{\rm d}+U_{\rm d})|}{U_{\rm d}\Gamma_{\rm N}}\}$ the diverging real part of $\Sigma_{1}(\omega)$ induces then a narrow Abrikosov–Suhl (or Kondo) peak at $\mu_{\rm N}$. From more sophisticated treatments it is known that at low temperatures its broadening should scale with $k_{\rm B}T_{\rm K}$. Unfortunately, the EOM approach does not reproduce the low energy structure of the Kondo peak. This missing information could be obtained, e.g., from renormalization group calculations [26, 37], but we nevertheless hope that the overall spectrum and the transport properties will be qualitatively properly reproduced by the present treatment.

In figure 7 we show the spectral function of a strongly correlated quantum dot obtained for $\varepsilon_{\rm d} = -2\Gamma_{\rm N}$, $U_{\rm d} = 10\Gamma_{\rm N}$ at $k_{\rm B}T = 0.0001\Gamma_{\rm N}$. The curve corresponding to $\Gamma_{\rm S} = 0$ (in the absence of the proximity effect) reveals the quasiparticle peak at $\varepsilon_{\rm d}$ and its Coulomb satellite at $\varepsilon_{\rm d} + U_{\rm d}$. Both peaks are broadened by $\sim\Gamma_{\rm N}$ (actually, the EOM approximation slightly overestimates this broadening). Besides the quasiparticle in-gap states we also notice a narrow Kondo resonance at $\omega = 0$.

For increasing values of the coupling $\Gamma_{\rm S}$ there occurs a gradual formation of particle and hole in-gap features (similar to what has been discussed in the previous sections). This process is accompanied by some qualitative changes of the Kondo resonance. It is gradually suppressed and for $\Gamma_{\rm S} \geq 4\Gamma_{\rm N}$ evolves to the kink-type structure characteristic

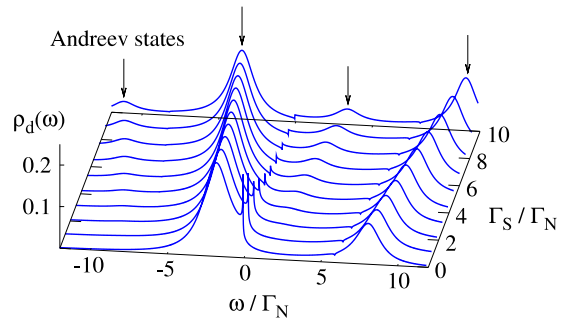

Figure 7. The spectral function $\rho_d(\omega)$ of a strongly correlated quantum dot obtained in the Kondo regime for $\varepsilon_d = -2\Gamma_N$, $U_d = 10\Gamma_N$ at temperature $T = 0.001\Gamma_N k_B^{-1}$ (well below T_K). The calculations have been made assuming Δ to be much larger than U_d.

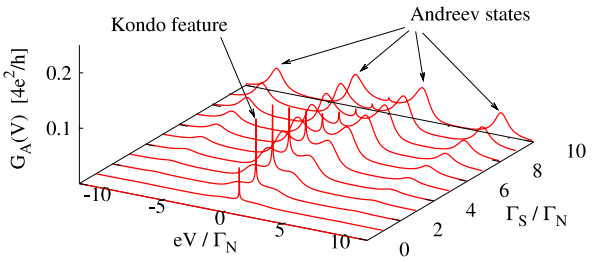

Figure 8. The differential Andreev conductance $G_A(V)$ of the Kondo regime obtained for the same model parameters as in figure 7. The zero-bias enhancement (caused by the Abrikosov–Suhl resonance) is gradually suppressed for increasing Γ_S due to the on-dot pairing.

for the mixed valence regime. This behavior is caused by the competition between the on-dot pairing (promoted by Γ_S) and the Kondo-type correlations [46]. Signatures of their eventual coexistence occur when Γ_S is comparable to or slightly larger than Γ_N. Under such conditions the subgap spectrum consists of four Andreev quasiparticle peaks (of a broadening $\sim\Gamma_N$) and a narrow Kondo resonance. These in-gap features can be practically observed by measurements of the differential conductance in the Kondo regime. The subgap conductance shown in figure 8 reveals all the mentioned peaks of the electronic spectrum (see figure 7) although in a symmetrized way, $G_A(V) = G_A(-V)$, because the particle and hole degrees of freedom participate equally in the Andreev scattering.

6. Conclusions

We have investigated the spectroscopic and transport properties of a quantum impurity coupled to one conducting and another superconducting electrode. The proximity effect depletes the electronic states in the subgap region $-\Delta < \omega < \Delta$ but Andreev-type scattering (i.e. conversion of electrons into Cooper pairs with a simultaneous reflection of the holes) contributes in-gap states, in both correlated and uncorrelated quantum dots. Since the Andreev mechanism involves the particle and hole degrees of freedom there appears an even number of in-gap bound states.

For a weak coupling to the metallic lead $\Gamma_N \ll \Gamma_S$ the in-gap states take the form of narrow resonances, representing infinite life-time quasiparticles. Otherwise, the in-gap states acquire a finite line-broadening, roughly proportional to Γ_N. The number of in-gap states depends sensitively on the Coulomb potential U_d (strictly speaking on the ratio U_d/Δ). For the weak interaction limit the ground state is preferred as the BCS singlet configuration [15, 28, 29], so consequently there appear only two Andreev subgap states. For stronger correlations $U_d \gg \Delta$ the number of in-gap states is doubled. The positions of these in-gap states depend on the ratio Δ/Γ_S. For $\Gamma_S \leq \Delta$ the in-gap states are located near the gap edge singularities $\sim\pm\Delta$. Otherwise, they move away from the gap edges and, in the extreme 'superconducting atomic limit' $\Gamma_S \gg \Delta$, the subgap quasiparticle energies approach $\pm\frac{1}{2}U_d \pm \sqrt{(\varepsilon_d + U_d/2)^2 + \Gamma_S^2/4}$. The coupling to the metallic lead merely affects the line-broadening of these in-gap states.

We have also studied the Kondo regime using an iterative scheme based on the equation of motion approximation [44]. In addition to the previously indicated Andreev states we have obtained a narrow Abrikosov–Suhl peak at $\omega = 0$. Such a Kondo feature is present in the spectrum unless a strong enough coupling to the superconducting lead Γ_S (promoting on-dot pairing) gradually suppresses it. In the region where the Kondo state coexists with the induced on-dot pairing the spectral function $\rho_d(\omega)$ is characterized by five subgap states: four of them represent the Andreev peaks (with a line-broadening $\sim \Gamma_N$) and the other one is due to the Abrikosov–Suhl resonance (with a broadening $\sim k_B T_K$). These features show up indirectly in the subgap conductance. Signatures of zero-bias enhancement of the Andreev conductance [5, 8, 23] can be naturally assigned to the Kondo effect. We hope that the present study discussing the influence of (i) the asymmetric couplings Γ_N/Γ_S, (ii) the energy gap Δ/Γ_S and (iii) the interplay between the Coulomb repulsion U_d and the induced on-dot pairing (promoted by Γ_S) will be useful for experimental studies of the many-body effects in N–QD–S junctions and in their more complex multi-terminal equivalents [12, 29, 37, 47, 48].

Acknowledgments

We acknowledge discussions with J Bauer, S Andergassen and K I Wysokiński and kindly thank R Aguado and Y Avishai for useful comments.

References

[1] Balatsky A V, Vekhter I and Zhu J-X 2006 *Rev. Mod. Phys.* **78** 373
[2] Anderson P W 1959 *J. Phys. Chem. Solids* **11** 26
[3] Abrikosov A A and Gorkov L P 1961 *Sov. Phys.—JETP* **12** 1243
[4] Luh Yu 1965 *Acta Phys. Sin.* **21** 75
Shiba H 1968 *Prog. Theor. Phys.* **40** 435
Rusinov A I 1969 *Sov. Phys.—JETP* **56** 2047
Shiba H and Soda T 1969 *Prog. Theor. Phys.* **41** 25
[5] Lee E J H, Jiang X, Aguado R, Katsaros G, Lieber C M and De Franceschi S 2012 *Phys. Rev. Lett.* **109** 186802

[6] Martín-Rodero A and Levy-Yeyati A 2011 *Adv. Phys.* **60** 899
[7] De Franceschi S, Kouwenhoven L, Schönenberger C and Wernsdorfer W 2010 *Nature Nanotechnol.* **5** 703
[8] Deacon R S, Tanaka Y, Oiwa A, Sakano R, Yoshida K, Shibata K, Hirakawa K and Tarucha S 2010 *Phys. Rev. Lett.* **104** 076805
Deacon R S, Tanaka Y, Oiwa A, Sakano R, Yoshida K, Shibata K, Hirakawa K and Tarucha S 2010 *Phys. Rev.* B **81** 121308
[9] Pillet J-D, Quay C H L, Morfin P, Bena C, Levy-Yeyati A and Joyez P 2010 *Nature Phys.* **6** 965
[10] Mourik V, Zuo K, Frolov S M, Pissard S R, Bakkers E P A M and Kouwenhoven L P 2012 *Science* **336** 1003
[11] Lee E J H, Jiang X, Houzet M, Aguado R, Lieber Ch M and Di Franceschi S 2013 (Preprint) arXiv:1302.2611v2
[12] Maurand R and Schönenberger Ch 2013 *Physics* **6** 75
Pillet J D, Joyez P, Žitko R and Goffman F M 2013 *Phys. Rev.* B **88** 045101
[13] Koerting V, Andersen B M, Flensberg K and Paaske J 2010 *Phys. Rev.* B **82** 245108
Andersen B M, Flensberg K, Koerting V and Paaske J 2011 *Phys. Rev. Lett.* **107** 256802
[14] Hübler F, Wolf M J, Scherer T, Wang D, Beckmann D and Löhneysen H v 2012 *Phys. Rev. Lett.* **109** 087004
[15] Bauer J, Oguri A and Hewson A C 2008 *J. Phys.: Condens. Matter* **19** 486211
[16] Hecht T, Weichselbaum A, von Delft J and Bulla R 2008 *J. Phys.: Condens. Matter* **20** 275213
[17] Beenakker C W J 1992 *Phys. Rev.* B **46** 12841
[18] Hofstetter L, Csonka S, Nygård J and Schönenberger C 2009 *Nature* **461** 960
[19] Herrmann L G, Portier F, Roche P, Levy Yeyati A, Kontos T and Strunk C 2010 *Phys. Rev. Lett.* **104** 026801
[20] Schindele J, Baumgartner A and Schönenberger C 2012 *Phys. Rev. Lett.* **109** 157002
[21] Hofstetter L, Geresdi A, Aagesen M, Nygård J, Schönenberger C and Csonka S 2010 *Phys. Rev. Lett.* **104** 246804
[22] Kim B-K, Ahn Y-H, Kim J-J, Choi M-S, Bae M-H, Kang K, Lim J S, Lopez R and Kim N 2013 *Phys. Rev. Lett.* **110** 076803
[23] Chang W, Manucharyan V E, Jaspersen T S, Nygård J and Marcus C M 2013 *Phys. Rev. Lett.* **110** 217005
[24] Vecino E, Martín-Rodero A and Levy Yeyati A 2003 *Phys. Rev.* B **68** 035105
[25] Martín-Rodero A and Levy Yeyati A 2012 *J. Phys.: Condens. Matter* **24** 385303
[26] Tanaka Y, Kawakami N and Oguri A 2007 *J. Phys. Soc. Japan* **76** 074701
[27] Wysokiński K I 2012 *J. Phys.: Condens. Matter* **24** 335303
[28] Meng T, Florens S and Simon P 2010 *Phys. Rev.* B **79** 224521
[29] Futturrer D, Swiebodzinski J, Governale M and König J 2013 *Phys. Rev.* B **87** 014509
Futturrer D, Governale M and König J 2010 *Europhys. Lett.* **91** 47004
[30] Fazio R and Raimondi R 1998 *Phys. Rev. Lett.* **80** 2913
Fazio R and Raimondi R 1999 *Phys. Rev. Lett.* **82** 4950
[31] Schwab P and Raimondi R 1999 *Phys. Rev.* B **59** 1637
[32] Krawiec M and Wysokiński K I 2004 *Supercond. Sci. Technol.* **17** 103
[33] Clerk A A, Ambegaokar V and Hershfield S 2000 *Phys. Rev.* B **61** 3555
[34] Cuevas J C, Levy Yeyati A and Martin-Rodero A 2001 *Phys. Rev.* B **63** 094515
[35] Yamada Y, Tanaka Y and Kawakami N 2011 *Phys. Rev.* B **84** 075484
[36] Avishai Y, Golub A and Zaikin A D 2001 *Phys. Rev.* B **63** 134515
Avishai Y, Golub A and Zaikin A D 2003 *Phys. Rev.* B **67** 041301(R)
Aono T, Golub A and Avishai Y 2003 *Phys. Rev.* B **68** 045312
[37] Oguri A, Tanaka Y and Bauer J 2013 *Phys. Rev.* B **87** 075432
[38] Domański T and Donabidowicz A 2008 *Phys. Rev.* B **78** 073105
Domański T, Donabidowicz A and Wysokiński K I 2008 *Phys. Rev.* B **78** 144515
Domański T, Donabidowicz A and Wysokiński K I 2007 *Phys. Rev.* B **76** 104514
[39] Karrasch C, Oguri A and Meden V 2008 *Phys. Rev.* B **77** 024517
Karrasch C and Meden V 2009 *Phys. Rev.* B **79** 045110
[40] Koga A 2013 *Phys. Rev.* B **87** 115409
[41] Kang K 1998 *Phys. Rev.* B **58** 9641
Cho S Y, Kang K and Ryu C-M 1999 *Phys. Rev.* B **60** 16874
[42] Sun Q-F, Wang J and Lin T-H 1999 *Phys. Rev.* B **59** 3831
Sun Q-F, Guo H and Lin T-H 2001 *Phys. Rev. Lett.* **87** 176601
[43] Levin K, Chen Q, Chien C-C and He Y 2010 *Ann. Phys.* **325** 233
Domański T and Ranninger J 2003 *Phys. Rev. Lett.* **91** 255301
[44] Meir Y, Wingreen N S and Lee P A 1991 *Phys. Rev. Lett.* **66** 3048
[45] Barański J and Domański T 2011 *Phys. Rev.* B **84** 195424
[46] Glazman L I and Matveev K A 1989 *Zh. Eksp. Teor. Fiz. Pis. Red.* **49** 570
Glazman L I and Matveev K A 1989 *JETP Lett.* **49** 659 (Engl. Transl.)
[47] Droste S, Andergassen S and Splettstoesser J 2012 *J. Phys.: Condens. Matter* **24** 415301
[48] Cottet A, Kontos T and Levy Yeyati A 2012 *Phys. Rev. Lett.* **108** 166803